

Low Index-Contrast Valley Hall Topological Photonics for Robust Transport in the Visible Spectrum

Pufan Liu,[†] Hongfei Zeng,[‡] David A. Czaplewski,[§] and Nathaniel P. Stern^{*,‡}

[†]Department of Materials Science and Engineering and [‡]Department of Physics and Astronomy, Northwestern University, Evanston, Illinois 60208, United States

[§]Center for Nanoscale Materials, Argonne National Laboratory, Argonne, Illinois 60439, United States

KEYWORDS: topological photonics, edge states, photonic crystal, nanophotonics, valley Hall

ABSTRACT: Topological photonics is an emerging platform to study light-matter interactions, with promising features such as robust edge state transmission that could be advantageous for quantum information applications. However, applying common topological photonic designs for visible wavelength light-matter interactions is challenging because materials compatible with the visible spectrum have lower refractive index contrasts. We design and demonstrate a novel valley Hall topological photonic crystal that can support a complete topological band gap in the visible spectrum. We also show an overetch procedure can be used to reduce the leakage loss common for low index contrast materials. To demonstrate these advantages, we fabricate topological photonic devices following these design principles and show that edge states at energies in the complete band gap have robust transmission around sharp corners. The compatibility of this photonic structure with straightforward fabrication methods will facilitate the study of interactions between topologically non-trivial photons and nanomaterials active in the visible spectrum.

Inspired by the recent advances in topological properties of matter^{1, 2}, topological photonics^{3, 4} aims to realize optical analogs of topological states of matter using photonic circuits. The non-interacting nature of photons is beneficial for long-distance transport of classical or quantum information⁵ and facilitates multiplexing multiple components into large-scale networks⁶. The versatility and technological maturity of photonic circuits bring advantages such as customizable design, easy fabrication, and flexible device integration schemes. Like its more familiar electronic counterpart, topological photonics presents several promising characteristics useful for other quantum studies. For example, topological edge states are protected from defect scattering, enabling lossless quantum information transmission^{5, 7} and robust optical delay lines^{8, 9}. The distributed optical coherence in topological photonics is a promising platform for exploring novel long-range entangled states¹⁰.

With these intriguing opportunities, understanding the details of how matter interacts with topological photonics will become increasingly important. For example, quantum superpositions generated by strong light-matter interactions can be transferred without loss by photons in a topological photonic circuit⁵. Interfacing matter with topological photonics can generate novel long-range light-matter hybrid states that leverage the directionality and delocalization of topological systems¹¹. Perhaps most interestingly, coupling of materials with light can provide topological photonic circuits with properties that are difficult to achieve with photonic circuits alone, such as strong magnetic responses and optical nonlinearities. Thus, the study of light-matter interactions in topological photonics can

both advance fundamental understanding of quantum optical systems and lead to practical applications such as fault-tolerant optical information processing¹².

Despite these motivations, there are so far very few studies of light-matter interactions in topological photonics¹³⁻¹⁵. The current dearth partially originates in a historical mismatch between the most convenient regimes for the components of this combination. Materials that show desirable properties for integration with topological photonics are typically found in the visible wavelength range. For example, transition metal dichalcogenides^{16, 17}, with intriguing strong spin-orbit coupling and non-trivial valley band structure, are active in the visible spectrum. In addition, photon counting, an essential technique to study the quantum optical features of light-matter interactions, is more efficient in the visible spectrum. In contrast, most of the well-recognized topological photonic structures¹⁸⁻²¹ are designed for telecommunications wavelengths and are poorly optimized for the visible spectrum. These geometries are not easily translatable to visible wavelength operation because the materials used for high refractive index contrast between the core layer and surrounding layers, such as silicon or gallium arsenide, usually have non-negligible absorption loss in the visible spectrum. Substituting materials with a lower index contrast but low visible absorption does not open a complete optical band gap, an essential condition to realize a viable topological photonic circuit (see Section S1 in the Supporting Information (SI) for details). So far, there are two existing approaches to make visible wavelength topological photonic structures. The first utilizes large footprint structures such as coupled ring resonator arrays⁹ or fiber arrays²², which have prob-

lems of either low operation bandwidth or difficulty in fabrication. The second achieves a higher index contrast with low-index core materials by altering the surrounding environment, such as removing the substrate²³. This more complicated fabrication is incompatible with standard scalable lithography procedures and adds significant challenges to assembling a structure with integrated materials for studying light-matter interactions.

In this work, we propose and demonstrate a novel topological photonic structure that can open a complete optical band gap in the visible spectral region using low index contrast materials compatible with standard silicon-based photonics fabrication procedures (silicon nitride (SiN) and silicon dioxide (SiO₂)). An overetch procedure is also designed to reduce the substrate leakage loss of the low index contrast configuration. This photonic structure is therefore suitable for integrating visible wavelength materials to study light-matter interactions in topological photonics. Although motivated by visible wavelength topological photonics, this structure can also be readily used in other wavelength ranges to reduce the need for high index contrast materials.

Topological properties do not often manifest experimentally in regions of topologically non-trivial order, but rather at the interface between regions with different topological order. In both topological electronics and photonics, conducting channels form at the boundary between two topologically distinct systems that in isolation both have an energy gap at this energy. Therefore, a common approach for designing topological photonics starts with a photonic crystal (PhC) with a gapless photonic band structure in which a band gap can be easily opened, such as one with Dirac cones in reciprocal space²⁰. The band gap at the Dirac points can be opened by selectively breaking certain symmetries of the original structure. For example, time-reversal symmetry can be broken to open the band gap with magnetic responses²⁴, optical nonlinearities²⁵, or temporal modulations²², and structural symmetries can also be broken to open the band gap by changing geometric properties of the structure¹⁸⁻²⁰. The second approach, such as valley Hall photonic topological insulators, is entirely based on the PhC geometry and does not require complex materials engineering. This removes material integration and fabrication challenges from the design of photonic structures themselves, promising a simpler approach when introducing other materials for studying light-matter interactions. Therefore, the topological structure proposed here for integrating visible materials builds on the valley Hall photonic topological insulator approach.

The base PhC for the proposed visible spectrum design is a hexagonal SiN PhC slab with circular holes on top of a planar SiO₂ substrate (Fig. 1a). Due to the $p6m$ plane group symmetry of this PhC, the transverse magnetic (TM) polarized modes have Dirac cones at the K points (Fig. 1e). For consistency with the experimental waveguide coupling to the PhC, TM modes in this manuscript are defined as the transverse magnetic electromagnetic mode traveling in a SiN waveguide, i.e., with major electric components out-of-plane. In the band diagram calculations for the PhC (Fig. 1e), the thickness of the SiN layer and the lattice constant,

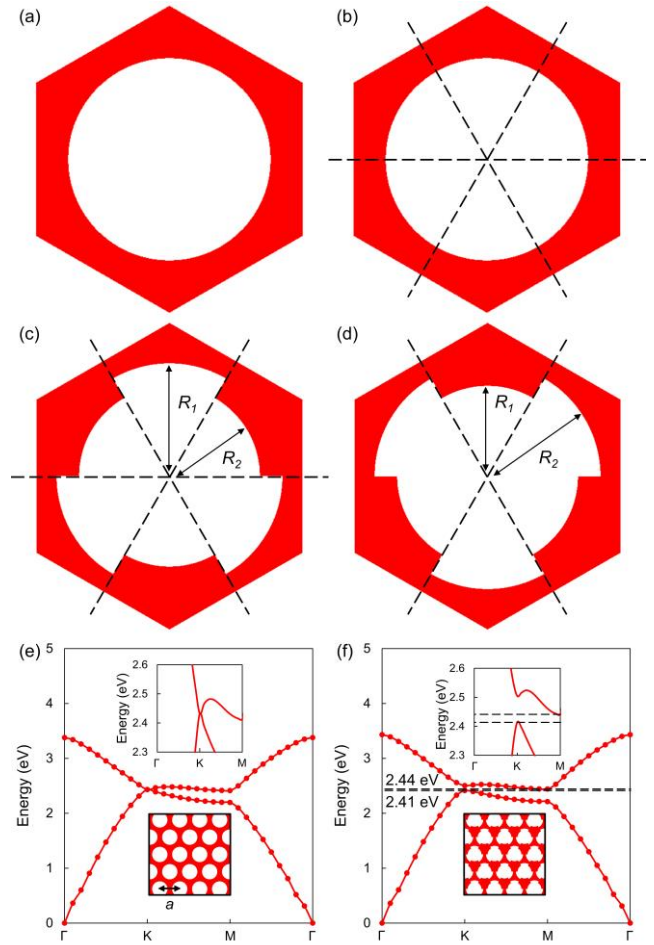


Figure 1: (a) Unit cell of a PhC with $p6m$ symmetry, which leads to Dirac cones at the K points in TM mode. The red region of the PhC is dielectric (SiN used in simulation and experiments) and the white region is air (in experiments, where SiN has been removed). (b) The unit cell is divided into six sectors. (c) The symmetry of the PhC is reduced to $p3m1$ by making the circular radius of each sector different, here with $R_1 = 0.425a$ and $R_2 = 0.34a$. (d) A complementary way to reduce the symmetry with $R_1 = 0.34a$ and $R_2 = 0.425a$. (e) Band diagram of the PhC given in a. Dirac cones are at the K points (inset). Radius of the circular air holes is $0.38a$. (f) Band diagram of the PhCs given in c and d. Black dashed lines depict the complete band gap. (Inset) Zoomed-in diagram near the band gap at the K points.

a , of the PhC are 238 nm and 220 nm, respectively. These specific numbers are chosen so the spectral results agree with the experiments discussed later in the text. The general features of the band structure do not depend strongly on the choice of these geometric parameters. To open a band gap in this base PhC, the symmetry is reduced by dividing the circular hole into six sectors and alternately increasing the radius of three of the sectors to R_1 and reducing the radius of the other three to R_2 (Fig. 1b, c). This reduces the plane group symmetry from $p6m$ to $p3m1$ and opens a band gap at the K points (Fig. 1f). The same symmetry breaking occurs by interchanging R_1 and R_2 (Fig. 1d). The PhCs of Fig. 1c and 1d are mirror images of each other, and therefore they have the same band structure shown in

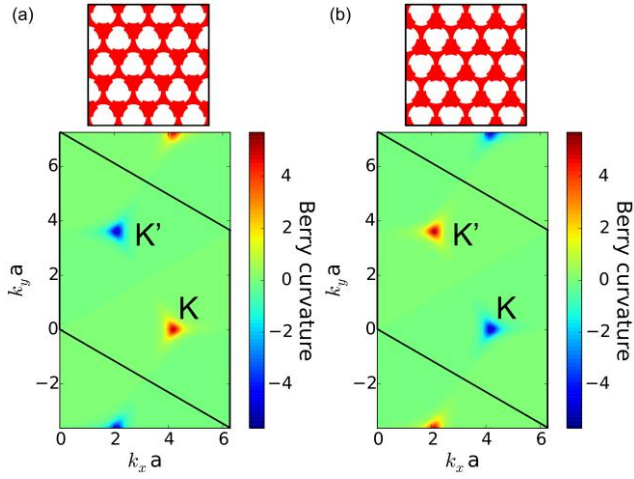


Figure 2: Berry curvatures of the PhCs given in (a) Fig. 1c and (b) Fig. 1d, with one Brillouin zone outlined by the solid line. The Berry curvature at each corresponding point in the two figures has the same magnitude but opposite sign. The magnitude is maximized at the band gap at the two inequivalent K points.

Fig. 1f. Despite this similar band structure, the Berry curvature near the band gap at the two K points (labeled as K and K') is opposite in sign for the two PhCs (Fig. 2). Therefore, it is impossible to continuously transform one PhC into the other, either by adjusting R_1 and R_2 or by rotation, without crossing the configuration where the Berry curvature vanishes and the band gap closes, i.e., the geometry where the plane group symmetry recovers to $p6m$ in the case of adjusting R_1 and R_2 and to $p31m$ in the case of rotation. Consequently, in analogy with other topologically non-trivial systems, spatially localized edge modes must appear inside the band gap at an interface between regions of PhCs with these two distinct geometries (see Section S2 in the SI for details on the character of these requisite edge states).

The above discussion motivates the existence of topological edge states at the interface of the two PhCs pictured in Fig. 1c and 1d. However, it does not guarantee the robustness of these edge states against defect scattering. The topological protection of edge states appears when photons have no modes of the same energy to scatter into (see Section S2 in the SI for discussion of edge state scattering). This requires opening a complete optical band gap of the PhC at the edge state energy. For the topological PhCs described above, the upper part of the band gap at the K points overlaps with the 2nd band near the M points (inset of Fig. 1f). While edge states must exist due to symmetry requirements, photons are not protected from scattering into bulk states near the M points. However, the lower part of the band gap noted by black dashed lines is complete, not overlapping with any other energy state for the entire reciprocal space; photons in this energy range will be protected from scattering. By increasing the radius of the larger sectors (assumed to be R_1), the upper band edge at the M points can be raised relative to the band at the K points, giving a larger bandwidth of the complete band gap (Fig. 3b). The radius of the smaller sectors, R_2 , is kept at $0.34a$ for these simulations since it is close to the optimized

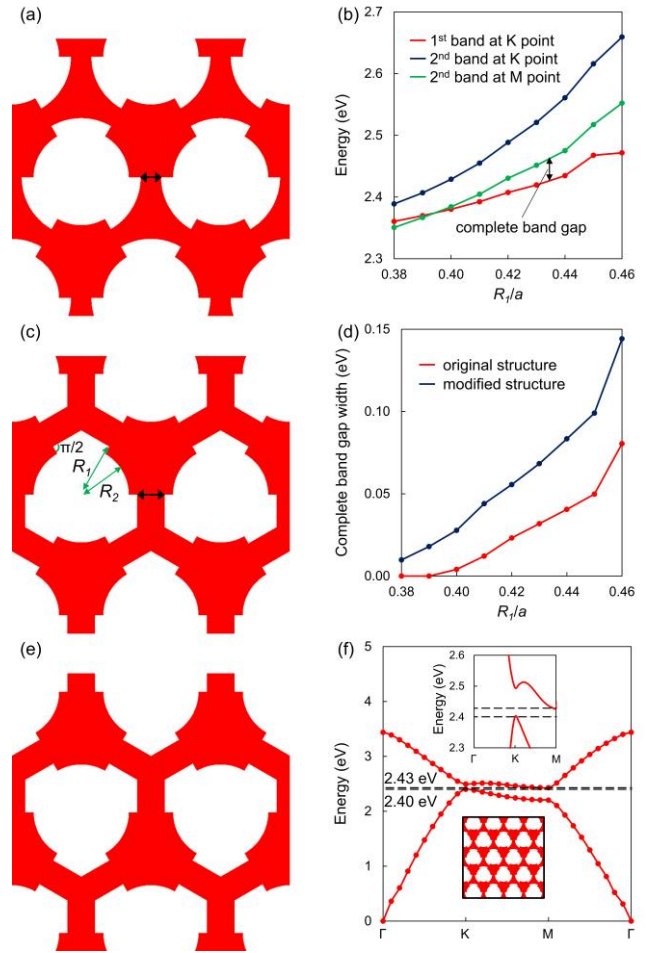


Figure 3: (a) PhC given in Fig. 1d. The black arrow shows the bridge between air holes that could have a high aspect ratio if R_1 is too close to $0.5a$. (b) Band edge energies of the PhCs given in Fig. 1c as a function of R_1 . R_2 is kept at $0.34a$. The complete band gaps between the 1st band at the K points and the 2nd band at the M points (indicated by arrows) grows in width as R_1 increases. (c) A modified PhC of Fig. 1c, in which the larger sectors are replaced with polygons. Here, $R_1 = 0.4a$ and $R_2 = 0.34a$. (d) Comparison of the complete band gap widths at each R_1 for the original PhC in Fig. 1c and the modified PhC in c. R_2 is kept at $0.34a$. The modified PhC can support similar larger complete band gap widths with smaller R_1 . (e) The reciprocal PhC to c, with R_1 and R_2 switched. (f) Band diagram of PhCs given in c and e. Black dashed lines depict the complete band gap. (Inset) Zoomed-in diagram near the band gap at the K points.

value for the largest complete band gap width for the ranges of R_1 used.

The above PhC design can in principle achieve topological edge modes at any reasonable wavelength, including the visible spectrum, for a suitable choice of geometric parameters. In practice, however, these PhCs can be challenging to fabricate if R_1 is close to $0.5a$, forcing the complete band gap to be small. For a PhC fabricated by electron beam lithography, the aspect ratio of the small bridge between two air holes noted by black arrows in Fig. 3a can become quite large if R_1 is close to $0.5a$, making the resist pattern mechanically unstable²⁶ and potentially resulting

in poor pattern transfer during fabrication. To overcome this challenge of high aspect ratio resist patterns, the PhC geometry is modified by replacing the larger sectors with polygons (Fig. 3c). With smaller R_1 and hence the smaller resist aspect ratio, the modified PhC can support similar complete band gap widths compared to the original PhC (Fig. 3d). Fig. 3f shows the band diagram of the modified PhC, with a complete band gap (labeled by black dashed lines). The modified PhC (Fig. 3c) and the associated PhC with R_1 and R_2 swapped (Fig. 3e) will be referred to as PhC A and PhC B, respectively. The previous arguments for topological edge modes still hold true for the modified PhCs, as none of the symmetries have been altered.

Although the origin of this topological photonic feature is primarily a two-dimensional phenomenon, the PhC design can be further optimized for realistic three-dimensional materials. Because it uses low index contrast materials SiN and SiO₂, light is not tightly confined inside the SiN layers of the PhC and there can be significant leakage loss into the air and the SiO₂ substrate. The band gap at the K points is well below the light cone of air, but it is in close proximity with the light cone of SiO₂ (Fig. 4a). Therefore, it is expected that small scattering centers can provide the momentum mismatch to scatter photons into the SiO₂ bulk modes. Such scattering losses can undermine loss-sensitive potential applications such as strong light-matter coupling or quantum information transport. To overcome this problem, we design an easy-to-implement overetch procedure illustrated in Fig. 4a to reduce the leakage loss in the PhC. By continuing to etch the structure after the SiN layer is depleted, the PhC pattern is partially transferred to the top of the SiO₂ substrate, significantly reducing scattering from topological edge modes. This overetch procedure achieves the reduced edge mode scattering without sacrificing properties beneficial for light-matter coupling such as high evanescent field leakage and single vertical mode operation.

3D finite-difference time-domain (FDTD) simulations on topological resonators (Fig. 5a) are used to illustrate this effect and identify the optimal overetch depth for real samples. The resonator consists of a triangular region of PhC A (labeled in gray, the side length of the triangular region is $19a$) and the surrounding region formed by PhC B (labeled in white). The edge state at their interface will form the boundary of a closed triangle. The electric field intensity map across the simulation region shows that the field is indeed concentrated at the triangular-shaped edge states (Fig. 5b). Since the edge states form a closed loop, the optical field at the resonance energies will be amplified due to constructive interference. The quality factors, Q , of the resonance modes can be used to quantify the internal losses of resonators and hence the effect of overetching.

To extract Q from numerical simulations, a Gaussian source with linear polarization aligned to couple only to the TM mode is injected at the edge of the resonator, and a monitor is placed at another position along the resonator edge mode. Since the convergence of a high- Q resonator simulation can take prohibitively long time in FDTD, the Q of a resonator mode is determined in a two-step procedure. First, broadband simulations are conducted at a reasonably short time scale, with the monitor collecting

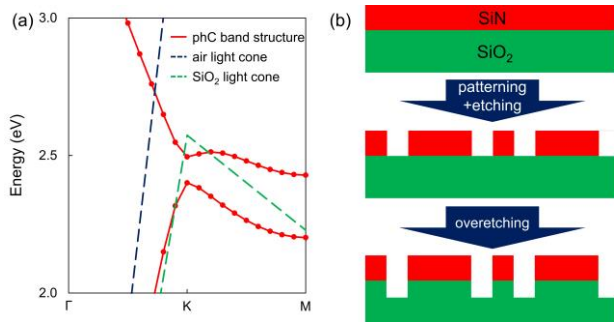


Figure 4: (a) Band diagram of PhC A, B near the K points compared with light cone borders of air and SiO₂. The band gap energies are far below the light cone of air but is in close proximity of the SiO₂ light cone. (b) Schematic diagram of the overetch procedure. The etch continues for some time after the SiN slab layer has been selectively removed, transferring part of the PhC patterns onto the SiO₂ substrate and breaking the SiO₂ bulk modes near the SiN layer.

frequency domain data to determine the energies of the resonance modes (Fig. 5c). At each resonant energy, a narrowband simulation is conducted on a reasonably short time scale, with the monitor collecting time domain data to determine the decaying envelop of the electric field. Q is extracted from the decay time for each mode.

The resonance mode inside the complete band gap has a higher Q than the one outside the complete band gap, implying that photons inside the complete band gap are indeed protected from scattering. The highest Q of each resonator structure within the topological band gap range is extracted as a function of overetch depth (Fig. 5d). The ∞ overetch depth data is obtained by extending the overetch region outside the simulation boundary, effectively assuming an overetch region extending to infinity. Three data sets are obtained for lattice constants $a = 220$ nm, 250 nm, and 280 nm, which are labeled by the resonance energies of the highest Q modes. For all three data sets, increasing the overetch depth increases Q , with the 2.42 eV and 2.19 eV data sets achieving $Q > 10,000$ with 400 nm overetch depth, which is more than half of the maximum Q possible with the ∞ overetch depth. If we explore the behavior as we adjust the photon energy, we find that reducing photon energies results in smaller Q at smaller overetch depths. The extreme case of the 2.00 eV data set has $Q < 5,000$ with 400 nm overetch depth, significantly less than the higher energy data sets for the same etch depth. The required overetch depth for a given Q does not scale linearly with a because the thickness of the SiN slab is kept constant (238 nm) across the simulations. With lower energy and hence larger wavelength, the fixed thickness SiN slab has worse light confinement, requiring more overetch depth to achieve a reasonably high Q . Therefore, applications that require a high Q at lower photon energies can be realized by starting with a SiN slab with larger thickness so that the required overetch depth can be kept less than 500 nm, which is readily achievable with high-selectivity etching recipes (See Section S3 in the SI for details). Applications at higher photon energies do not have the confinement problem and can reach high Q with the current SiN thickness.

These results demonstrate that the novel topological

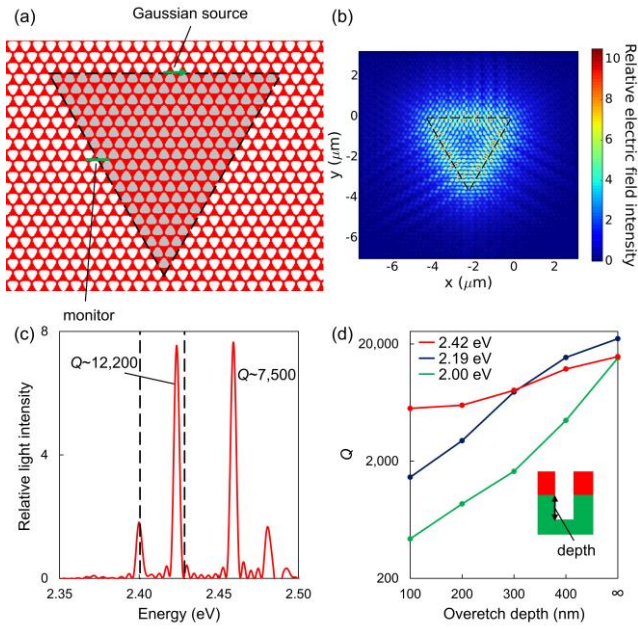


Figure 5: (a) Schematic of the simulated resonator structure. Structures in gray regions are PhC A and white regions are PhC B. The black dashed lines depict the path of the edge states. The positions of the injection source and monitor used in FDTD simulations are labeled in green arrow/line. (b) Simulated electric field intensity at one of the resonance energies of the triangular resonator. The electric field profile follows the triangular shaped edge state paths noted by black dashed lines as in a. (c) Broadband simulation of the relative light intensity received by the monitor with 400 nm overetch depth. At two major resonance modes, Q extracted from the narrowband simulations are labeled. As expected, the Q of the mode inside the complete band gap labeled by black dashed lines are larger than the other mode. (d) The highest Q of all the resonance modes inside the topological band gap of a resonator structure as a function of the overetch depth. The ∞ data point is realized by extending the overetch region outside the simulation boundary. The resonance energy is changed by adjusting a from 220 nm (red) to 250 nm (blue) and to 280 nm (green). For all three resonance energies, increasing the overetch depth can increase Q . Higher resonance energy allows a reasonable Q to be reached with lower overetch depth.

PhC design opens a complete optical band gap for visible wavelengths that can support robust edge state modes. The leakage loss of the edge state modes into the SiO_2 substrate can be effectively reduced using an overetch procedure with reasonable depth. This design avoids the need for fabricating a suspended PhC for larger index contrast such as was utilized in Ref. 23, therefore removing design constraints and fabrication challenges for integrating topological photonic circuits with visible-spectrum optical materials.

In order to demonstrate the existence and robustness of topological edge modes in the proposed PhC, photonic circuits based on the design are fabricated and measured. PhC devices are fabricated from a low-pressure-chemical-vapor-deposition stoichiometric $\text{SiN}/\text{SiO}_2/\text{Si}$ wafer. The thickness of the SiN and SiO_2 layers are 238 nm and 2,000 nm, respectively. The details of the fabrication, including

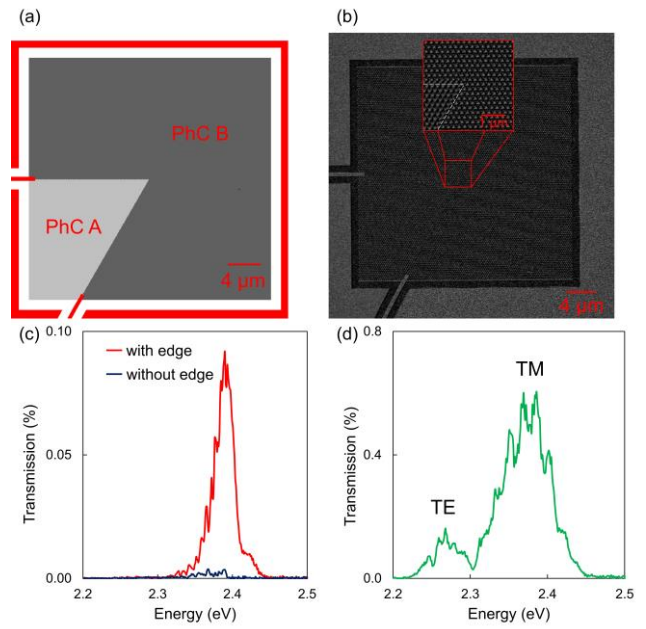


Fig. 6: (a) Schematic diagram of a typical fabricated device. The PhC device is connected to two waveguides which lead to two gratings for coupling in and out. (b) SEM image of one of the fabricated devices with $a = 220$ nm. The white dashed line depicts the path of the edge states. (c) Comparison of the measured transmission spectra of the device in a and a reference device having the same geometry as a but both regions are PhC A. The former shows a very clear transmission with a sharp peak profile, whereas the latter shows minimal transmission with no distinct spectral peak. See Section S4 in the SI for details. (d) Measured transmission spectra of the gratings used. The edge state transmission measured from c overlaps with the TM mode transmission of the gratings but is narrower in linewidth, with no transmission observed in the TE spectral region of the gratings.

the etch recipes for the overetch procedure, are given in Section S3 in the SI. The PhC device is composed of two regions of PhC A and PhC B geometries, with the boundary between them making a 120° kink (Fig. 6a,b). The PhC A/PhC B boundary starts at one 500-nm wide SiN waveguide, makes a 120° turn, and continues to another SiN waveguide. The turn is used to suppress unintended collection of forward scattered light, which will not follow a sharp turn like the propagating edge state. Each of the waveguides terminates in a remote grating coupler for input or output to the circuit. The polarization dependence of the gratings allows selective coupling of the TM mode into the waveguide and PhC device while using an unpolarized white light source. The device is measured by coupling light between single mode fibers and the circuit using the grating couplers. Unpolarized light from a white light source is launched into the input fiber and the signal in the output fiber is collected.

The transmission spectrum of the device (referenced to the unpolarized white light source used) is compared with that of a reference device in which both PhC regions have the same PhC A geometry and which therefore has no boundary and no topological edge mode. The topological device shows a strongly peaked transmission spectrum,

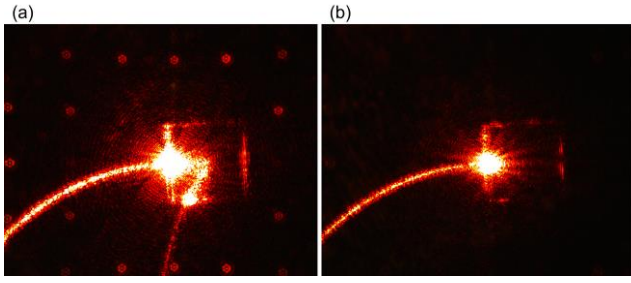


Figure 7: (a) Image taken when the laser source is inside the band gap of PhC, i.e., at 627 nm. A clear edge state transmission that follows the corner edge path expected from Fig. 6a can be seen. Scattered light on input and output comes from the mode mismatch between edge modes and waveguide modes. See Section S4 in the SI for details. (b) Image taken when the laser source is slightly outside the band gap of PhC, i.e., at 617 nm. No obvious transmission through the edge state to the outcoupling waveguide can be seen.

whereas the reference device has lower transmission consistent with scattered background rather than edge mode transmission (Fig. 6c). The transmission spectrum of the grating couplers obtained from a simpler device consisting of two grating couplers connected by a waveguide shows that the gratings couple at different wavelengths for transverse electric (TE) and TM modes (Fig. 6d). Comparing the PhC device and grating transmission spectra, the transmission of the topological photonic device is only significant for the wavelengths of the TM mode, and it is narrower than the grating TM mode transmission. This, together with minimal transmission of the reference device without PhC boundaries, suggests that the transmission spectrum in Fig. 6c comes from topological edge states.

In order to further show that this transmission belongs to edge states, a photonic circuit is simultaneously imaged while light is coupled into the circuit to observe the scattered light (See Section S5 in the SI for details). A topological photonic device is fabricated with the PhC band gap centered at 1.98 eV (627 nm) and with a long 2.5 cm waveguide length connecting the PhC device and the input grating. The long waveguide allows both the input fiber and imaging objective to be simultaneously positioned above the sample. The PhC structure is analogous to that shown in Fig. 6a except that $a = 280$ nm. A white light source is used to locate the position of the PhC device. Once located, the white light source is turned off and a monochromatic laser source is sent into the grating through single-mode fiber and the device is imaged from above. When the laser wavelength is within the topological band gap (627 nm, Fig. 7a), light is seen along the PhC boundary, following the 120° turn and continuing in the output waveguide, confirming the presence of an edge mode. When the laser wavelength is outside the topological band gap (617 nm, Fig. 7b), however, no light is seen along the PhC device and output waveguide, eliminating scattering as a cause of the transmission in the angled edge mode (Fig. 6c). The objective can image the topological edge mode even though the band gap is outside the air light cone because sidewall roughness scatters a minimal yet observable amount of light into the light cone that can be collected through the objective.

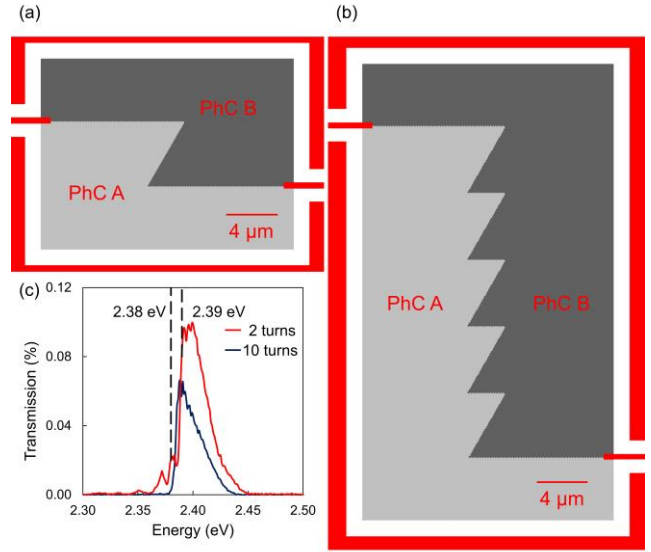


Figure 8: (a-b) Schematic diagrams of fabricated devices with multiple turns during the edge state path, where a has two turns and b has ten turns. (c) Measured transmission spectra of the two devices with $a = 220$ nm in configurations outlined in a and b. The transmission is lower for the ten-turn device outside the complete band gap noted by black dashed lines, but it is comparable inside the complete band gap. See Section S4 in the SI for details.

The robust transmission of the edge states is experimentally confirmed using devices with multiple 120° turns. Representative schematic diagrams are shown in Fig. 8a, b for devices with two and ten turns, respectively. Measured spectra show that when the number of turns is increased, the transmission at higher energy drops, while transmission at lower energy is essentially unchanged (Fig. 8c). This distinct behavior across the spectrum is explained by the PhC band structure (Fig. 3f). The lower energy region of the edge state near the K points is in a complete band gap and is protected against scattering, but the higher energy region of the edge mode is not in a complete band gap and is susceptible to scattering into bulk modes. Even though the fabricated devices do not perfectly match the design, evidenced by a lower band gap energy and a smaller complete band gap width compared to expectations from Fig. 3f, they experimentally demonstrate that a complete band gap can be opened at visible wavelengths using this design and the resulting edge states have robust transmission minimally impacted by direction changes.

In summary, we have designed a novel visible-wavelength topological PhC that is compatible with standard silicon-based photonics fabrication procedures using low index contrast materials (SiN and SiO₂). The in-plane loss of the resulting topological edge states is minimized by opening a complete band gap, and the out-of-plane loss is minimized through an overetch procedure. Topological photonic devices following this design have been fabricated and evaluated via transmission and imaging experiments. These results demonstrate the existence of topological edge states and the robustness of edge states against scattering. The benefits of this topological photonic design

can advance the study of light-matter interactions in the visible wavelength range.

ASSOCIATED CONTENT

Supporting Information

Additional details of photonic topological insulator design and fabrication procedures are available free of charge on the ACS Publication website.

AUTHOR INFORMATION

Corresponding Author

* Email: n-stern@northwestern.edu

Notes

The authors declare no competing financial interest.

ACKNOWLEDGMENT

This work was supported as part of the Center for Molecular Quantum Transduction, an Energy Frontier Research Center funded by the U.S. Department of Energy, Office of Science, Basic Energy Sciences under Award #DE-SC0021314. Use of the Center for Nanoscale Materials, an Office of Science user facility, was supported by the U.S. Department of Energy, Office of Science, Office of Basic Energy Sciences, under Contract No. DE-AC02-06CH11357.

REFERENCES

1. Ando, Y., Topological Insulator Materials. *Journal of the Physical Society of Japan* 2013, 82 (10), 102001.
2. Hasan, M. Z.; Kane, C. L., Colloquium: Topological Insulators. *Reviews of Modern Physics* 2010, 82 (4), 3045.
3. Lu, L.; Joannopoulos, J. D.; Soljačić, M., Topological Photonics. *Nature Photonics* 2014, 8 (11), 821-829.
4. Ozawa, T.; Price, H. M.; Amo, A.; Goldman, N.; Hafezi, M.; Lu, L.; Rechtsman, M. C.; Schuster, D.; Simon, J.; Zilberberg, O., Topological Photonics. *Reviews of Modern Physics* 2019, 91 (1), 015006.
5. Blanco-Redondo, A.; Bell, B.; Oren, D.; Eggleton, B. J.; Segev, M., Topological Protection of Biphoton States. *Science* 2018, 362 (6414), 568-571.
6. Ishio, H.; Minowa, J.; Nosu, K., Review and Status of Wavelength-Division-Multiplexing Technology and Its Application. *Journal of Lightwave Technology* 1984, 2 (4), 448-463.
7. Mittal, S.; Fan, J.; Faez, S.; Migdall, A.; Taylor, J. M.; Hafezi, M., Topologically Robust Transport of Photons in a Synthetic Gauge Field. *Physical Review Letters* 2014, 113 (8), 087403.
8. Cheng, X.; Jouvaud, C.; Ni, X.; Mousavi, S. H.; Genack, A. Z.; Khanikaev, A. B., Robust Reconfigurable Electromagnetic Pathways within a Photonic Topological Insulator. *Nature Materials* 2016, 15 (5), 542-548.
9. Hafezi, M.; Demler, E. A.; Lukin, M. D.; Taylor, J. M., Robust Optical Delay Lines with Topological Protection. *Nature Physics* 2011, 7 (11), 907-912.
10. Wen, X.-G., Topological Order: From Long-Range Entangled Quantum Matter to a Unified Origin of Light and Electrons. *International Scholarly Research Notices* 2013, 2013.
11. Barik, S.; Karasahin, A.; Flower, C.; Cai, T.; Miyake, H.; DeGottardi, W.; Hafezi, M.; Waks, E., A Topological Quantum Optics Interface. *Science* 2018, 359 (6376), 666-668.
12. Yao, X.-C.; Wang, T.-X.; Chen, H.-Z.; Gao, W.-B.; Fowler, A. G.; Raussendorf, R.; Chen, Z.-B.; Liu, N.-L.; Lu, C.-Y.; Deng, Y.-J., Experimental Demonstration of Topological Error Correction. *Nature* 2012, 482 (7386), 489-494.
13. Klembt, S.; Harder, T.; Egorov, O.; Winkler, K.; Ge, R.; Bandres, M.; Emmerling, M.; Worschech, L.; Liew, T.; Segev, M., Exciton-Polariton Topological Insulator. *Nature* 2018, 562 (7728), 552-556.
14. Guddala, S.; Komissarenko, F.; Kiriushchikina, S.; Vakulenko, A.; Li, M.; Menon, V.; Alù, A.; Khanikaev, A., Topological Phonon-Polariton Funneling in Midinfrared Metasurfaces. *Science* 2021, 374 (6564), 225-227.
15. Li, M.; Sinev, I.; Benimetskiy, F.; Ivanova, T.; Khestanova, E.; Kiriushchikina, S.; Vakulenko, A.; Guddala, S.; Skolnick, M.; Menon, V., Experimental Observation of Topological Exciton-Polaritons in Transition Metal Dichalcogenide Monolayers. *arXiv preprint arXiv:2009.11237* 2020.
16. Manzeli, S.; Ovchinnikov, D.; Pasquier, D.; Yazyev, O. V.; Kis, A., 2d Transition Metal Dichalcogenides. *Nature Reviews Materials* 2017, 2 (8), 1-15.
17. Wang, G.; Chernikov, A.; Glazov, M. M.; Heinz, T. F.; Marie, X.; Amand, T.; Urbaszek, B., Colloquium: Excitons in Atomically Thin Transition Metal Dichalcogenides. *Reviews of Modern Physics* 2018, 90 (2), 021001.
18. He, X.-T.; Liang, E.-T.; Yuan, J.-J.; Qiu, H.-Y.; Chen, X.-D.; Zhao, F.-L.; Dong, J.-W., A Silicon-on-Insulator Slab for Topological Valley Transport. *Nature Communications* 2019, 10 (1), 1-9.
19. Shalaev, M. I.; Walasik, W.; Tsukernik, A.; Xu, Y.; Litchinitser, N. M., Robust Topologically Protected Transport in Photonic Crystals at Telecommunication Wavelengths. *Nature Nanotechnology* 2019, 14 (1), 31-34.
20. Wu, L.-H.; Hu, X., Scheme for Achieving a Topological Photonic Crystal by Using Dielectric Material. *Physical Review Letters* 2015, 114 (22), 223901.
21. Goralach, M. A.; Ni, X.; Smirnova, D. A.; Korobkin, D.; Zhirihin, D.; Slobozhanyuk, A. P.; Belov, P. A.; Alù, A.; Khanikaev, A. B., Far-Field Probing of Leaky Topological States in All-Dielectric Metasurfaces. *Nature communications* 2018, 9 (1), 1-8.
22. Rechtsman, M. C.; Zeuner, J. M.; Plotnik, Y.; Lumer, Y.; Podolsky, D.; Dreisow, F.; Nolte, S.; Segev, M.; Szameit, A., Photonic Floquet Topological Insulators. *Nature* 2013, 496 (7444), 196-200.
23. Liu, W.; Hwang, M.; Ji, Z.; Wang, Y.; Modi, G.; Agarwal, R., Z2 Photonic Topological Insulators in the Visible Wavelength Range for Robust Nanoscale Photonics. *Nano Letters* 2020, 20 (2), 1329-1335.
24. Wang, Z.; Chong, Y.; Joannopoulos, J. D.; Soljačić, M., Observation of Unidirectional Backscattering-Immune Topological Electromagnetic States. *Nature* 2009, 461 (7265), 772-775.
25. Hadad, Y.; Khanikaev, A. B.; Alu, A., Self-Induced Topological Transitions and Edge States Supported by Nonlinear Staggered Potentials. *Physical Review B* 2016, 93 (15), 155112.
26. Tanaka, T.; Morigami, M.; Atoda, N., Mechanism of Resist Pattern Collapse During Development Process. *Japanese Journal of Applied Physics* 1993, 32 (12S), 6059.

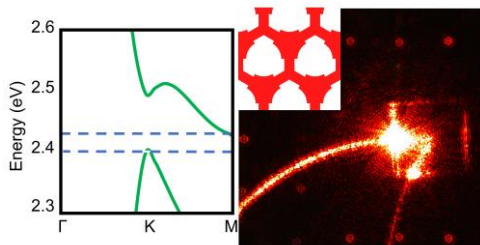
For Table of Contents Use Only

Low Index-Contrast Valley Hall Topological Photonics for Robust Transport in the Visible Spectrum

Pufan Liu,[†] Hongfei Zeng,[‡] David A. Czaplewski,[§] and Nathaniel P. Stern^{*,‡}

[†]Department of Materials Science and Engineering and [‡]Department of Physics and Astronomy, Northwestern University, Evanston, Illinois 60208, United States

[§]Center for Nanoscale Materials, Argonne National Laboratory, Argonne, Illinois 60439, United States



Please find our TOC figure above. The left panel shows the band diagram of our designed topological photonic crystal (PhC) in this manuscript, which features a complete topological band gap in visible wavelength range, a characteristic that is necessary to suppress scattering during edge state transmission. The right panel shows the imaging result of one of the topological PhC devices we fabricated, which shows the light transmission through the edge state. The inset of the right panel shows the geometry of the designed PhC.